Extracting Implosion Velocity and Compression from Self-Emission Radiography in Direct-Drive Inertial Confinement Fusion

Ruojian F. Li

Webster Thomas High School

Webster, NY

Advisor: Dr. Luke Ceurvorst

Laboratory for Laser Energetics

University of Rochester

Rochester, NY

Month 2024

1. Abstract

In direct-drive inertial confinement fusion implosions, benchmarking simulations is critical for ensuring their reliability. In this work, an automated program was developed using MATLAB to determine the position of the target shell at various times. Using images of the x-rays emitted by the target at different implosion times, an Abel inversion, a function used in image analysis to extract emission as a function of radius from a scanned image, was applied. These profiles were further used to extract the emission edge position of the target by taking the midpoint of the emission function's rising edge. Previous 1D LILAC simulations were then benchmarked by comparing the experimentally determined positions to the simulated positions, confirming the validity of the program. This program can be used when new simulations are made for alternative target materials as it is important to understand how energy is coupled between the laser and the target. By comparing experimentally determined positions from the program to simulated positions, the accuracy of the alternate material simulations can be inferred.

2. Introduction

2.1 Inertial confinement fusion

Inertial confinement fusion (ICF) is a method of fusion where fusion is achieved by compressing a capsule of fuel to extreme densities and temperatures. At the Laboratory for Laser Energetics (LLE), this is done through direct drive, high-energy lasers are uniformly directed at the surface of a spherical cryogenic target, compressing the deuterium-tritium (DT) fuel. The process of direct drive ICF is summarized in Figure 1, showing the four main stages of a target implosion. At early times [Fig 1(a)], the laser is absorbed by the target, which leads to the ablation of the target surface, this transforms the surface of the target into plasma. This plasma rapidly expands outward, and by Newtons third law, this creates a rocket effect, driving the fuel of the target inwards[1]. Rayleigh-Taylor instabilities [Figure 1(b)] are outside of the scope of this work and will not be discussed in this paper. As the implosion progresses, it reaches a deceleration phase [Figure 1(c)]. During the deceleration phase, the kinetic energy of the imploding shell is converted into thermal energy, and the DT fuel is compressed and heated[1]. Peak compression, or stagnation, occurs in the final stage [Figure 1(d)]. In stagnation, a central hot spot begins to form, with temperature and density conditions extreme enough for fusion reactions to occur[1]. In order for fusion to occur, the conditions must reach extreme high temperature and density conditions. The maximum temperature of the hot spot is dependent on the kinetic energy of the shell, and therefore, the faster a target is imploded at, the more fusion reactions, and therefore more energy it will yield[2].

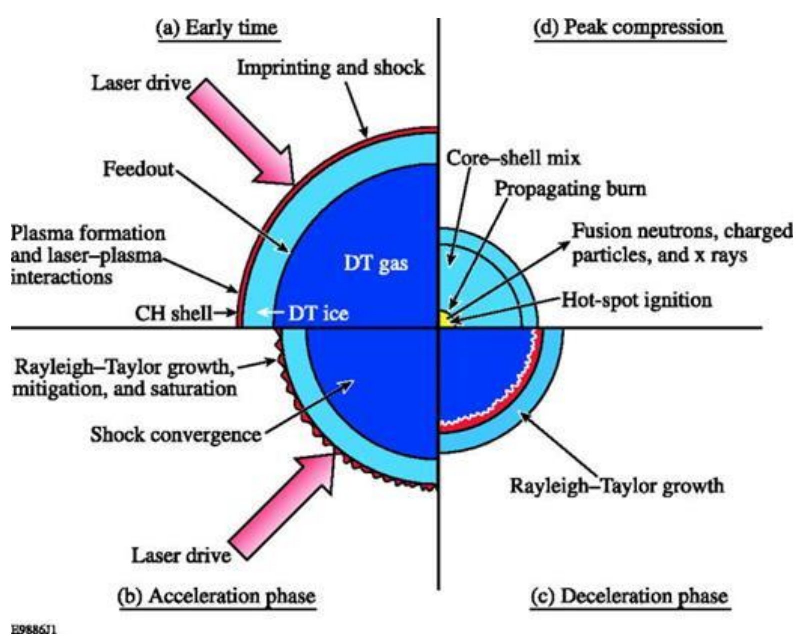

Figure 1. The four main stages of direct-drive ICF (a) The laser is absorbed by the target, leading to ablation. (b) Not relevant to study. (c) The shell is decelerating; kinetic energy is converted into thermal energy. (d) At peak compression a hot spot forms, where fusion occurs. From Ref. 1

Knowing this, it is paramount that the ablator material is able to effectively absorb the energy from the laser for maximum shell kinetic energy.

2.2 Energy coupling in alternate materials

As previously mentioned, an ICF target is composed DT fuel surrounded by an ablator. The ablator's primary function is to absorb energy from the laser and convert it into kinetic energy, this is done via a rocket effect from the expanding plasma. This conversion from laser energy to kinetic energy is known as energy coupling. In order to enhance energy coupling, ablators are often doped with various materials. Doping is where amounts of different atoms are added to material in order to modify the material's properties. In both the National Ignition Facility (NIF) and LLE, different ablators have been tested, and it has been concluded that different ablators result in different energy couplings and yields[3]. On the OMEGA laser, silicon dopants have previously been tested. Figure 2 shows a sector of silicon doped target's initial conditions in the best preforming OMEGA shot (shot 104949). Experiments on the silicon doped target [Figure 2] concluded that the addition of a silicon dopant to the ablator enhanced collisional absorption[4].

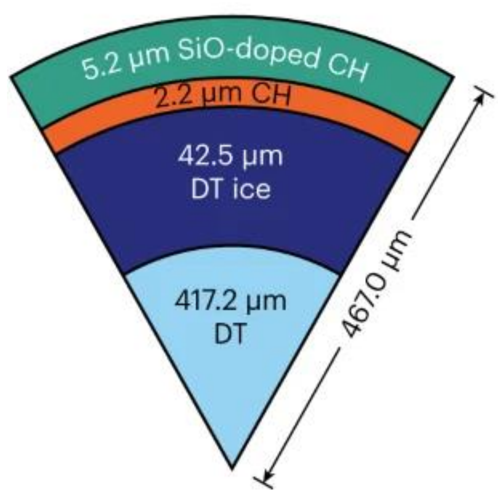

Figure 2. A sector of a Silicon doped ICF target. The target is composed of 2 layers of DT fuel, surrounded by 2 layers of ablator. From Ref. 4

The implosion velocity, and therefore fusion yield is dependent on the energy coupling from laser to kinetic energy, and since different materials couple energy differently, it is important to find a material with optimal energy absorption.

2.3 Simulations

In ICF research, having accurate simulation models is paramount to success. This is because simulations are fundamental to both designs, and understand implosions. To this end, it is important to be able to benchmark these simulations to ensure that their predictions can be evaluated with confidence. This can be done by determining the trajectory of the target as it implodes, and comparing it to simulated target trajectories. If the trajectories agree, and therefore the implosion velocities agree, it can be assumed that the energy coupling between the laser and the target was correctly modeled in the simulation. Simulation work like this has been done to benchmark the NIF's CBET model[5]. Being able to correctly model the energy dynamics of an implosion is fundamental, especially when experimenting with alternate ablator materials. However, when alternate target materials are introduced, it is fundamental that accuracy is maintained, in order to easily design and understand their implosions.

2.4 Self-emission and imaging

In order to benchmark simulations, it is key to understand self-emission and imaging in order to accurately extract the implosion trajectory. Self-emission has been continually utilized to visualize implosions, allowing for a myriad of information to be extracted. Previously, self-emission has been utilized on OMEGA to provide evidence for low mode drive asymmetry[6]. Self-emission occurs when a region is hot and dense. In an ICF target, the ablation front is where the target begins to get hot, where the material ablates off the cold surface, which expands outwards and pushes the other material inwards. As the laser is absorbed in the absorption region, and heat is transferred to the ablation front via electrons in thermal conduction. Because the ablation front is where self-emission starts, because it is where the target begins to get hot, tracking the positions of the ablation front using time resolved self-emission imaging is a prominent method to obtain the implosion trajectory and velocity. The time resolved self-emission images can be taken by framing cameras, which consists of individually timed strips that acquire data when a pulse travels through it, this pulse takes time to travel across the strip, which yields a time difference of 50 picoseconds between frames. Using time-resolved self-emission imaging will be paramount to this study, as it will be fundamental to extracting the trajectory of an implosion.

3. Algorithm

3.1 Data Preparation

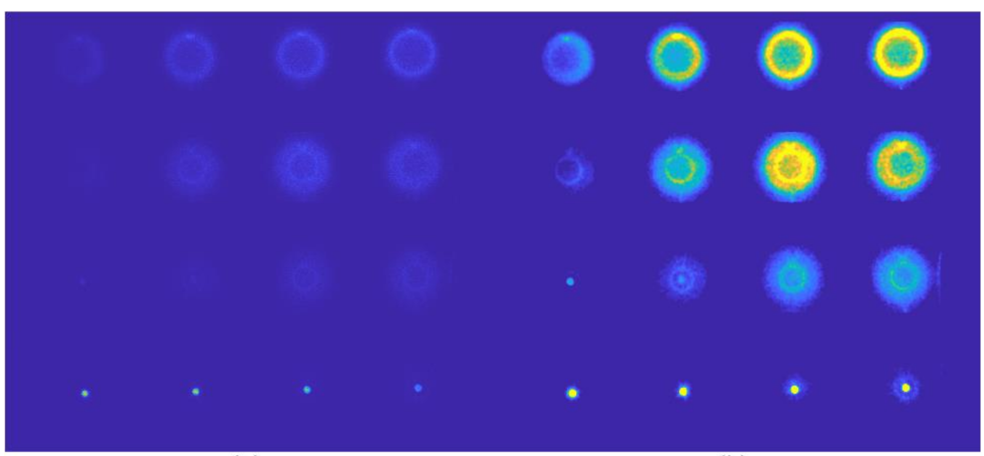

Figure 3. Side by side comparison of raw data (a) and "smoothed data" (b), this data is read right left, top down. When the data is "smoothed" there is less noise, and a greater contrast between the target and its surroundings.

The input of the program is an image depicting 4 strips of 4 frames of self-emission x-ray images taken from the framing camera. In figure 3, the left [Figure 3(a)] shows the raw scanned data, with very low contrast between the target and the surroundings, this data is read chronologically right-left, top-down. In order to output the smoothed data on the right, a built in imadjust function was first applied, which adjusts the intensity values of the image to enhance contrast. In conjunction with this, a built in medfilt2 function was applied, which performs median filtering on the image, which is a noise reduction technique. By replacing each pixel's value with the median of the pixel values in its surrounding region, medfilt2 is able to smooth out noise while keeping a circular shape. In order to further prepare this data for analysis, each circle was isolated. To begin this process, the program splits the smoothed data into an equal sized 4x4 grid, and outputs 16 sub images containing each of the circles. Now, each of these sub images can be individually worked with.

3.2 Circle detection and correction

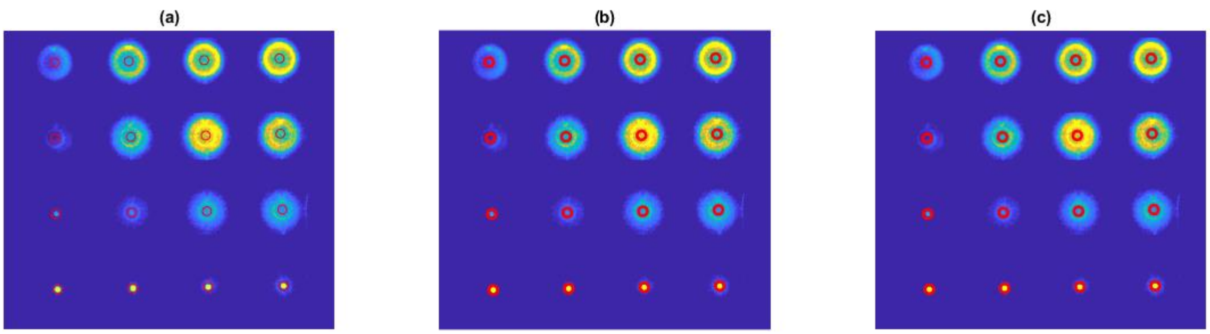

Figure 4. Smoothed data, overlapped with red circles depicting: (a) initial detected centers. (b) fit grid. (c) corrected centers. By comparing (a) to (b), (c) is outputted when the difference between (a) and (b) is greater than a threshold distance.

Using the 16 equal sized sub images, the next step was to find the center of each of the circles, in order to later unwrap them into polar coordinates. The program iterated through every sub image, utilizing a built in MATLAB function imfindcircles with function sensitivity loop, which determines how sensitive the function is to detecting circles, with a higher sensitivity correlating to a higher likelihood of detecting a circle, but having a higher likelihood to detect a false positive, if more than one circle was detected, then the sensitivity was lowered in order to decrease the likelihood of a false circle, and vice versa for if no circles were detected. By following this iterative process, the code was able to detect exactly one circle per sub image. Figure 4(a) shows the smoothed data overlapped with these detected centers, shown in red. It can be observed that these detected centers are not exactly centered on each circle. So, in order to increase robustness and remove outliers, a fit function was applied. Using the initial detected circles position, a fit function was applied in order to create a 4x4 grid of equally separated points, this was done by creating a linear model for the x and y positions. Figure 4(b) shows the fit grid; as expected, these points are equally spaced in the y and x directions. Finally, the grid and initial center positions were compared to output the final circle positions [Figure 4(c)]. It was found that a threshold of 5 pixels was an optimal maximum distance between two corresponding points in the grid and the original set of centers. If a point was found to be over 5 pixels in distance from the corresponding grid point at the same index, the center position was simply changed to the grid value. Iterating through the new center positions, a sub image was cropped about the center position from the original data for each of the circles.

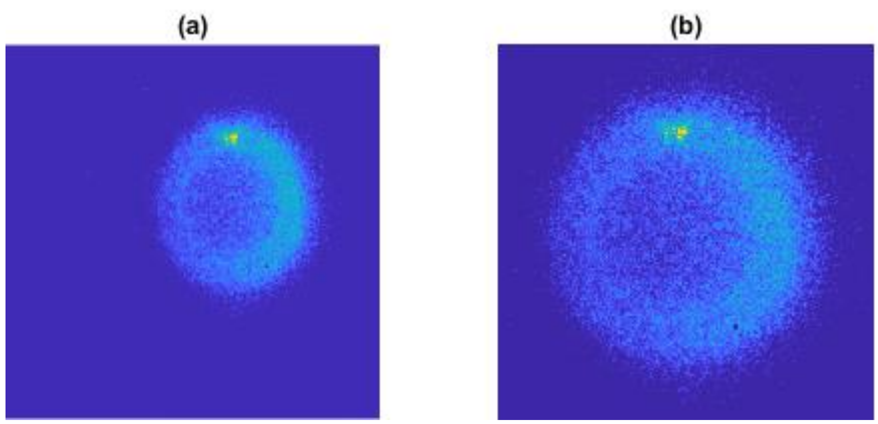

Figure 5. Side by side comparison between (a) sub image (resized) from data preparation (3.1) and (b) sub image from circle detection. After circle detection, the centered sub image is fully prepared to be analyzed.

Figure 5 shows a side-by-side comparison between the sub image [figure 5(a)] from data preparation (3.1) and sub image [figure 5(b)] from circle detection. The next step is to convert the data from Cartesian to polar coordinates, so taking this circle detection step is important in order to center the image at the circle center. After this is done, where there are 16 sub images centered at each of the center positions, then the data can finally be unwrapped, and further analyzed.

3.3 Trajectory

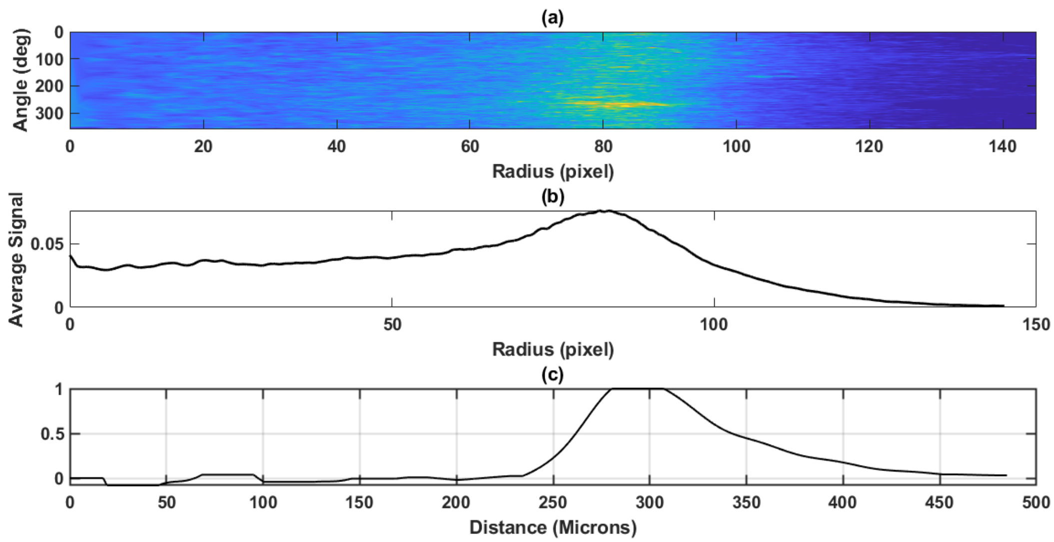

Figure 6. Graphs extracted from self-emission imaging at 2.78ns. (a) Data converted to polar coordinates. (b) Average signal from the data over radius. (c) Radial profile extracted from an Abel Inversion of (b).

In order to extract the position of the emission edge for each of the individual sub images, a radial emission profile must be constructed in order to extract where the position is. In order to do this, the program iterated through every centered sub image and unwrapped the image from cartesian to polar coordinates, plotting the angle vs radius. Figure 6 shows the steps leading to extracting the radial profile at time 2.78ns. Figure 6(a) shows the unwrapped image, with angle in degrees plotted against radius in pixels. Taking this unwrapped image, the average signal over radius was taken [figure 6(b)]. This was done while ignoring the emission from the stock- the thing that holds the target. The stock can be observed from around 270-290 degrees, and has a distinct yellow color in the unwrapped graph.

With yellow indicating high emission as the stock gets very hot, it is important to ignore the data there. Taking the average profile, an Abel inversion can be applied to find the underlying radial function of the sub image. The Abel Inversion [Equation 1], is a function that is used in image analysis that is used to calculate the emission function of a scanned image of the emission function[7]. In this case, low attenuation and perfect spherical symmetry is assumed, allowing for the Abel Inversion to be utilized. Using a prewritten Abel Inversion function on MATLAB[8], an emission profile was extracted [Figure 6(c)].

$$f(r) = -\frac{1}{\pi}\int_r^\infty \frac{dF}{dy}\frac{dy}{\sqrt{y^2 - r^2}}$$

Equation 1. Abel Inversion, a function used to calculate the emission function of a scanned image of the emission.

In order to extract the emission edge position for the trajectory, an assumption was made that this was positioned at the midpoint of the rising edge of the emission profile. By finding the trough through the built in findpeaks function, and finding where the radial profile crosses the midpoint between the trough and the max (The Abel inversion is normalized, so the max is always 1) in the rising edge, the emission edge position can be extracted by the program. The normalized Abel Inversion graph [figure 6(c)] is in microns, while the figures 6(a) and 6(b) are in pixels. In order to convert from pixels to microns, the pixel size was determined, achieved by calculating the magnification factor, derived from the physical distance between features in the image (in microns) and their corresponding distance in pixels, and adjusted using the magnification. Iterating through every sub image, unwrapping the image, averaging it, applying the Abel Inversion, and detecting the midpoint, the position at each time and therefore the trajectory can be determined.

4. Program Assessment

4.1 Simulation Comparison

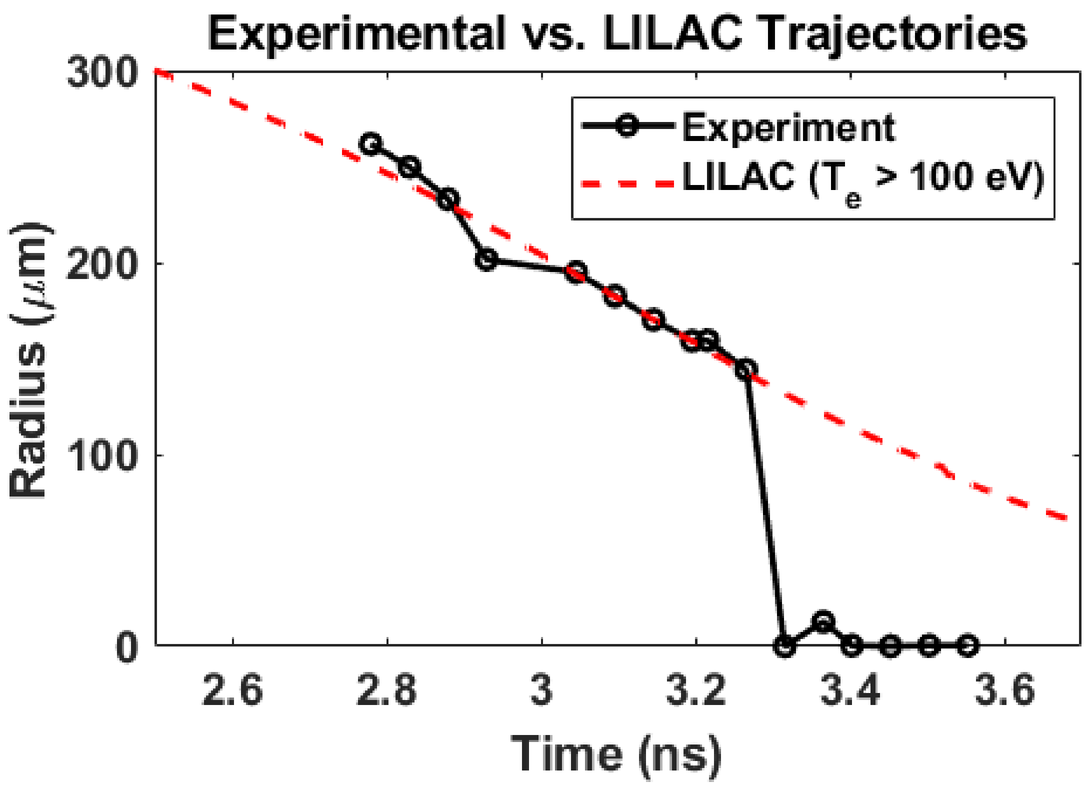

Figure 7. Experimental trajectories vs LILAC Trajectories. There is good agreement between the two until ~3.3 ns, where a hot spot begins to form in the core of the target.

Figure 7 shows a graph of radius vs time, in microns and nanoseconds, respectively. In black is the program's measured times, with the circles showing where the images were taken. In red, is a simulated trajectory taken from 1D LILAC simulations, a 1-dimensional hydrocode[1], of when the electron temperature first exceeded 100 eV. It can be observed that there is good agreement between the simulated and measured trajectories until ~3.3 nanoseconds. This occurs at stagnation, where the hot spot begins to form from pressure-volume work. This hot spot becomes very bright and overcomes the ablation-front signal, and quickly become the only signal because of the limited dynamic range of the detector- the detector has a limited range between the minimum and maximum emission signal. This program was tested against 3 other self-emission image sets and produced good results every time. From this, it can be concluded that this program is functional and is a new way to both benchmark simulations and provide automatic data for new and historical data for experiments.

4.2 Future improvements

There can be other improvements that can be made to expand the robustness of the program, including a more robust automation of the circle detection. More automation can be made to adjust the minimum circle radius detected from the imfindcircles function. As it is very difficult to predict when a hot spot is going to form, it has been a challenge to implement an automatic method to input the minimum circle size, as inputting to large of a circle radius would yield no results, while inputting too small of a circle radius could yield false circles from noise. Other than adjustments in the automation and robustness of the code, there is not yet a quantitative way to compare the simulated and measured trajectories. Therefore, it is important to implement error bars to the measured trajectory graph in the future. Error bars can be derived from the slope of the rising edge of emission, with a higher slope correlating to a lower margin of error. With error bars, the reliability of simulations can fully be determined, giving a quantitative way to compare simulations with measured trajectories.

5. Conclusion

In this work, an automated program was created to extract the trajectory of the emission edge of an ICF implosion using time-resolved self-emission imaging. Using techniques such as Hough shape detection and Abel Inversions, the trajectories were found, and used to compare to their corresponding 1D LILAC simulations. Simulations are important tools in experiments are they are used both to design and understand implosions. Using this program will be a useful tool for benchmarking programs, and will help gain a better understanding of energy coupling in implosions. This is especially prominent when testing out new ablator materials. In March of 2025, this program will be utilized to test Germanium doped ablators and benchmark their simulations.

6. Acknowledgements

First, I would like to thank my adviser, Dr. Ceurvorst for all his help, support, and most notably, his patience. With his guidance, I was able to learn and understand code for the first time. He helped me do this faster than I thought I was capable of learning. Next, I would like to thank both Dr. Craxton and Ms. Truebger for helping to put together this wonderful research opportunity and making sure it ran as smoothly as possible. Also, I would like to thank all of the guest seminar speakers for expanding my science knowledge to new horizons every week. Additionally, I would to thank everyone at IT for all of the help with my VPN issues. Lastly, I would like to thank each and every one of my fellow high school students, for their contributions to a motivating, positive work environment.

7. References

1. R. S. Craxton, K. S. Anderson, T. R. Boehly, V. N. Goncharov, D. R. Harding, J. P. Knauer, R. L. McCrory, P. W. McKenty, D. D. Meyerhofer, J. F. Myatt, A. J. Schmitt, J. D. Sethian, R. W. Short, S. Skupsky, W. Theobald, W. L. Kruer, K. Tanaka, R. Betti, T. J. B. Collins, J. A. Delettrez, S. X. Hu, J. A. Marozas, A. V. Maximov, D. T. Michel, P. B. Radha, S. P. Regan, T. C. Sangster, W. Seka, A. A. Solodov, J. M. Soures, C. Stoeckl, J. D. Zuegel; Direct-drive inertial confinement fusion: A review. *Phys. Plasmas* 1 November 2015; 22 (11): 110501. https://doi.org/10.1063/1.4934714

2. P. B. Radha *et al*., "Inertial Confinement Fusion Using the OMEGA Laser System," in *IEEE Transactions on Plasma Science*, vol. 39, no. 4, pp. 1007-1014, April 2011, doi: 10.1109/TPS.2011.2109949. keywords: {Electric shock;Ignition;Shape;Laser fusion;Measurement by laser beam;Silicon;Confinement;direct drive;fusion;inertial},

3. O L Landen et al 2008 J. Phys.: Conf. Ser. 112 022004

4. Gopalaswamy, V., Williams, C.A., Betti, R. *et al.* Demonstration of a hydrodynamically equivalent burning plasma in direct-drive inertial confinement fusion. *Nat. Phys.* **20**, 751–757 (2024). https://doi.org/10.1038/s41567-023-02361-4

5. P. B. Radha, M. Hohenberger, D. H. Edgell, J. A. Marozas, F. J. Marshall, D. T. Michel, M. J. Rosenberg, W. Seka, A. Shvydky, T. R. Boehly, T. J. B. Collins, E. M. Campbell, R. S. Craxton, J. A. Delettrez, S. N. Dixit, J. A. Frenje, D. H. Froula, V. N. Goncharov, S. X. Hu, J. P. Knauer, R. L. McCrory, P.

W. McKenty, D. D. Meyerhofer, J. Moody, J. F. Myatt, R. D. Petrasso, S. P. Regan, T. C. Sangster, H. Sio, S. Skupsky, A. Zylstra; Direct drive: Simulations and results from the National Ignition Facility. *Phys. Plasmas* 1 May 2016; 23 (5): 056305. https://doi.org/10.1063/1.4946023

6. Shah, R. C., Haines, B. M., Wysocki, F. J., Benage, J. F., Fooks, J. A., Glebov, V., Hakel, P., Hoppe, M., Igumenshchev, I. V., Kagan, G., Mancini, R. C., Marshall, F. J., Michel, D. T., Murphy, T. J., Schoff, M. E., Silverstein, K., Stoeckl, C., & Yaakobi, B. (2017). Systematic fuel cavity asymmetries in directly driven inertial confinement fusion implosions. *Physical Review Letters, 118*(13), 135001. https://doi.org/10.1103/PhysRevLett.118.135001

7. Ma, S., Gao, H., Wu, L., & Zhang, G. (2008). Abel inversion using Legendre polynomials approximations. *Journal of Quantitative Spectroscopy and Radiative Transfer, 109*(10), 1745-1757. https://doi.org/10.1016/j.jqsrt.2008.01.013

8. Carsten Killer (2024). Abel Inversion Algorithm (https://www.mathworks.com/matlabcentral/fileexchange/43639-abel-inversion-algorithm), MATLAB Central File Exchange. Retrieved September 2, 2024.

9. Delettrez, J., Epstein, R., Richardson, M. C., Jaanimagi, P. A., & Henke, B. L. (1987). Effect of laser illumination nonuniformity on the analysis of time-resolved x-ray measurements in uv spherical transport experiments. *Physical Review A, 36*(8), 3926-3934. https://doi.org/10.1103/PhysRevA.36.3926